Spring 5-12-2018

DETECTION OF SALEN-TYPE TRACERS FOR SUBTERRANEAN FLUID FLOW MONITORING USING SURFACE-ENHANCED RAMAN SPECTROSCOPY

Jenny C. Sanchez
University of New Mexico

Jenny C. Sanchez
Candidate

Chemistry and Chemical Biology
Department

This thesis is approved, and it is acceptable in quality and form for publication:

Approved by the Thesis Committee:

Richard A. Kemp, Chairperson

Terefe G. Habteyes

Ramesh Giri

DETECTION OF SALEN-TYPE TRACERS FOR SUBTERRANEAN FLUID FLOW MONITORING USING SURFACE-ENHANCED RAMAN SPECTROSCOPY

by

JENNY C. SANCHEZ

B.S., NEW MEXICO STATE UNIVERSITY, 2004

THESIS

Submitted in Partial Fulfillment of the
Requirements for the Degree of

Master of Science
Chemistry

The University of New Mexico
Albuquerque, New Mexico

May, 2018

DEDICATION

This work is lovingly dedicated to my little sister, Vivian.

ACKNOWLEDGEMENTS

I gratefully acknowledge my co-advisors, Dr. Richard Kemp and Dr. Terefe Habteyes, for their support and patience during my time working on this research project. Dr. Kemp, it is an honor to have become your final graduate student, thank you for allowing me the opportunity. You helped me achieve something that at times I never imagined I could. Dr. Habteyes, you are a kind and motivating advisor, thank you for including me in your group and sharing your knowledge with me. Lastly, I would like to thank Dr. Ramesh Giri for being on my thesis committee and for teaching me organometallic chemistry with the enthusiasm in which you did.

I would like to thank the members of the Habteyes group for their friendship and for their willingness to always help me, you were fundamental in forming my graduate experience. 'Professor Tefera', your kindness and time spent teaching and helping me will never be forgotten. I wish you the greatest success in your life. I would like to thank former member of the Kemp group, Orion, for his camaraderie- you will make a fine chemist one day. I would also like to acknowledge the research group of Dr. Timothy Boyle for their significant contributions to this work.

This thesis became a reality with the kind support from many cherished friends and esteemed coworkers at the Air Force Research Laboratory, thank you for your constant support. Rachel and Stephanie, thank you for being a source of encouragement, for

reminding me to have confidence in myself, and to never give up without a fight. Your support at the very end will always be a reminder of the true meaning of friendship.

To my mom Ana, thank you for your unconditional love and boundless faith in my abilities, I hope I have made you proud.

Finally, Shawn. You have been so supportive throughout this educational pursuit of mine. Thank you for perpetually believing in me, for always reminding me it would all be worth it, for your companionship during the really long days and late nights, and for keeping me and Bucky alive during the final stages of this journey. For this and more, you are forever in my heart and I am eternally grateful that life brought us together.

DETECTION OF SALEN-TYPE TRACERS FOR SUBTERRANEAN FLUID FLOW MONITORING USING SURFACE-ENHANCED RAMAN SPECTROSCOPY

by

Jenny C. Sanchez

B.S., Biology, New Mexico State University, 2004
M.S., Chemistry, University of New Mexico, 2018

ABSTRACT

A series of hydrocarbon and aqueous soluble salen-type ligands have been synthesized and characterized by electronic and vibrational spectroscopy. Aqueous soluble salen-type ligands were complexed to a metal and investigated as potential underground fluid flow tracers using Surface-Enhanced Raman Spectroscopy (SERS) as the analytical technique. Vibrational spectra obtained from SERS was shown to have enhanced the spectral signal for these complexes in low concentrations though did not show significant differences between the free ligands and their metal complexes. This research has shown that, with some structural modifications, salen-type ligands can be effective candidates as subterranean fluid flow tracers when SERS is used as the detection method. Findings also suggest that SERS is a potentially suitable technique for the above ground detection of underground fluid flow tracers, though additional work is needed to improve the specificity of detection of this analytical technique.

TABLE OF CONTENTS

LIST OF FIGURES

LIST OF TABLES

1. Introduction

1.1. Background

The majority of the energy consumed in the United States is derived from non-renewable fossil fuels such as petroleum, coal, and natural gas.[1] To a lesser extent it is derived from renewable sources such as hydropower and geothermal, although the long-term outlook for growth in renewable energy generation and consumption is forecasted to significantly increase, according to the U.S. Energy Information Administration.[1] Given that energy is the nation's most fundamental resource, it has become vital to safeguard access to these non-renewable and renewable sources and equally essential to maintain a supply of energy. Therefore, to ensure U.S. energy security there has been a growing focus to maximize oil recovery and geothermal power.

To meet the growing national energy demand, energy production has become a priority for the United States, which has become the largest producer of petroleum, natural gas, and geothermal power, globally.[2] Energy produced from these sources is largely acquired by utilizing a technology known as hydraulic fracturing. Hydraulic fracturing, a method used since the 1940s, produces fractures in rock formations thousands of feet below the Earth's surface. This is achieved by pumping high pressure fluid down drilled wells to create and enlarge fractures in the earth, thereby stimulating the flow of energy sources such as hydrocarbon or geothermal heat stored deep within, increasing the volumes that can be recovered. Hydraulic fracturing fluids consist of water, proppants, and chemical additives that work together to create and

maintain the pathways that subsequently increase the rate which energy sources are released from the underground reservoir formations. It is the proppants, materials such as sand, ceramics, or other constituents, that hold open the newly created fractures.[3]

Hydraulic fracturing is credited for the sizeable increase in U.S. energy production and the technology has evolved significantly as a result of research and development efforts.[4] Although this technology has advanced considerably, there is a gap in the industry's ability to measure hydraulic fracturing reservoir performance, which results in inefficiencies during energy production and difficulties in predicting future production from reservoirs.[5] With industrial energy producers uniformly forecasting an increase in energy consumption both nationally and globally, this represents a problem that requires a solution.

1.2. Objective

Efficient and cost-effective production of subterranean reservoir fluids (hydrocarbon and aqueous) is dependent on detailed information about fluid flows from fractured areas. A visual representation of a typical horizontal shale oil well is shown in Figure 1.

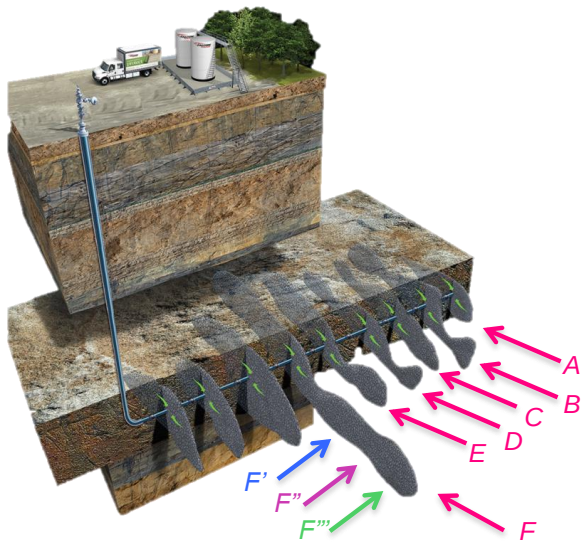

Figure 1: A Typical Horizontal Shale Oil Well and Zones

Figure 1 illustrates how partitioned zones are created by the hydraulic fracturing process along a pre-drilled horizontal portion of a well (zones A-F). The ability to confidently identify if a particular zone is producing fluid is critical to maximizing the efficiency of a hydraulic fracturing process in addition to potentially resolving difficulties that may arise during production, especially since flow patterns are not predictable and are changeable over time. Currently there are methods of monitoring subterranean fluid flows but each have disadvantages that compromise the reliability of the information. One method employs the use of fluorescent molecules as dyes, many of which are thermally stable though they have been reported to adsorb onto reservoir rock.[6] Radioactive species have been widely used as tracers and have been particularly useful but due to radiation hazards their use has lessened.[6] Safety concerns aside, there are an insufficient number of these species which limit the amount of zones that can be monitored. Another method still under development is

the use of DNA fragments, which offer the possibility of an infinite number of unique markers that can be designed but present difficulties as a reliable quantitative method as they have been found unable to withstand the harsh pressure, temperature, and/or chemical conditions that can be encountered at subterranean conditions. Therefore the need for an effective tracer system that is safe, cost-effective, and provides unlimited and unique identifiers that can characterize flow patterns from many specific areas in underground reservoirs is appropriate for investigation.[6] One such method can be utilized using a chemical approach. Controlled chemical tracer methods are proving successful for characterizing some hydraulic properties and for flow path identification, but also have been successful in the characterization and estimation of chemical transport processes and properties.[7] A promising tracer method, based on chemical molecular species, able to qualitatively determine the source of the fluid, i.e. identifying which fracture zone or a sub-zone (Figure 1, F'-F''') the product is coming from is investigated herein.

Molecular species containing a chelating agent able to bind to any metal (M) are conceptually an ideal choice for a tracer primarily due to the number of available metal ions in existence and subsequently in the amount of complexes able to be formed. In particular, if the chelating agent is multidentate it offers the added benefit of increased stability due to the chelate effect. Due to the fact that the stability of a chelated complex depends on the size of the chelate rings formed, an ideal candidate should also form a chelate ring consisting of multiple atoms bound to the metal. For these reasons, Schiff bases with these set of characteristics are suitable candidates.

Schiff bases, discovered in 1864 by Hugo Schiff, are derived from the condensation reaction between a carbonyl compound and a primary amine.[8] Schiff bases coordinate to a range of metal ions via the imine nitrogen and at least one other group, usually linked to the carbonyl compound.[8] In this investigation an [O, N, N, O] tetradentate Schiff base ligand (L) was synthesized, following literature methods, by reacting two equivalents of salicylaldehyde with a diamine.[9] This particular ligand is commonly known as a salen, which is a contraction for salicylaldehyde and ethylenediamine. Although the term salen was used originally only to describe the tetradentate Schiff bases derived from the starting reactants salicylaldehyde and ethylenediamine, the more general term salen-type is used in the literature to describe the class of [O,N,N,O] tetradentate bis-Schiff base ligands.[10] The pre-organized cyclic structure of the Salen ligand donor atoms [O,N,N,O] also contribute to the stability of the molecule by minimizing additional strain on the ligand upon coordination.[11] This type of stability is a particularly significant characteristic considering effective tracers should not modify the physical properties of the reservoir fluids it is monitoring.[6] Of note is the ease and affordability by which these salen-type ligands and their complexes can be synthesized, also making them suitable for tracers. These complexes are also an attractive system to work with since the ligand backbone can be easily modified.[12] Lastly, salens and their derivatives can be complexed to a range of metals making the number of available distinguishable tracers very high.[13]

To be able to be a well-rounded tracer for underground fluid flows, selection criteria exist. In addition to some that have been mentioned in the previous section such as

stability, ease of synthesis, and affordability, the tracers must be soluble in both hydrocarbon and aqueous media.[6] In general, salens are hydrocarbon soluble and as such, present limited solubility in aqueous solutions.[12] To overcome this limitation and achieve broad solubility, modifications can be made to the ligand by introducing lipophilic and ionic substituents.[12,14]

The technical approach to using molecular species as tracers is to leverage the proppants in the hydraulic fracturing fluid. As stated earlier, proppants are components of hydraulic fracturing fluids. The main function of proppants is to keep open the fissures created during the hydraulic fracturing process. Originally sand was used as a proppant but modern proppants are mostly ceramics-based and range in size, geometry, and weight. All three of these properties can be tailored to perform in a variety of underground conditions and optimized to maintain fissures open to extract resources from the earth. Modern proppants are also coated with a variety of polymers that aim to provide a plentitude of advantages such as chemical, mechanical, and thermal stability enhancement.[15] Therefore, the approach to this research is to examine if salen-type metal-ligand (ML) complexes incorporated into controlled-release coated porous proppants can offer long term underground fluid flow monitoring capabilities. There are numerous types of proppants and coatings being developed, representing a growing field in the industry, however research is still needed to improve multifunctional proppant elution profiles and extend the lifetime of chemically infused proppants.[15]

Specifically, the objective of this research is to investigate salen-type ligands that have been synthesized and tuned to be soluble in either hydrocarbon or aqueous medium to determine if they can be used as distinguishable tracers providing fluid flow monitoring during hydraulic fracturing operations. This objective will be achieved by using Raman spectroscopy as the analytical technique that will identify these ligands, above ground. In addition to this qualitative aspect of the research it is a secondary goal to use a specialized type of Raman spectroscopy, Surface-Enhanced Raman Scattering (SERS), to determine if these molecules can be detected at very low concentrations. This will help determine if this approach is a feasible method to derive quantitative information about fluid flows. Background to the spectroscopy will be discussed in the following section.

1.3. Spectroscopy

Molecular spectroscopy is an investigative technique that obtains and explains information on molecular structure, dynamics, and other characteristics by measuring the interaction between matter and electromagnetic radiation.[16] Of the numerous spectroscopic techniques in existence, vibrational spectroscopy is particularly useful due to it being a non-destructive technique that provides unique, fingerprint-like spectra useful for molecular identification and therefore suitable to achieve the primary objective of this research. When light interacts with matter, the photons in the light can either be absorbed and/or scattered.[17] Absorption occurs if all, or a range, of the energy of the incident light is resonant with the vibrational frequencies of the atoms and any unabsorbed light will be transmitted. Scattering occurs when

light is dispersed or refracted upon interaction with the atoms and this occurs in all directions. The intensity of the scattered light is inversely proportional to the fourth power of the wavelength so a shorter wavelength incident laser will yield more scattering.[18] This scattering is said to be elastic if the frequency of the incident and scattered light is unchanged and inelastic if there is a change in frequency. If the scattering is elastic, the process is called Rayleigh scattering and if the scattering is inelastic, the process is called Raman scattering. In vibrational spectroscopy, transitions between molecular vibrational states can be measured via absorption as is done with Infrared (IR) spectroscopy or via scattering of light energy as is done with Raman spectroscopy. Although both of these vibrational spectroscopic techniques complement each other, the primary difference between each technique lies in the electronic characteristic of the molecular vibration. Upon excitation of a molecule, IR spectroscopy depends on a periodic change in the permanent dipole moment of that molecule and Raman spectroscopy depends on the change in polarizability of that molecule.[19] Polarizability is a property that describes how easily the electron cloud of a molecule may be distorted, creating an induced dipole, as a result of an electric field interaction.[20] This distinguishing feature is relevant to this research as the salen ligands under investigation are electron-rich and polarizable, thus perfect candidates for Raman spectroscopic investigation.

Raman spectroscopy is an inelastic scattering technique used for molecular identification. Raman spectroscopy is performed by exciting a molecule using monochromatic light followed by the measurement of the resulting scattered light.

Light, or electromagnetic radiation visible to the human eye, is characterized by its wavelength (λ). In spectroscopy, the wavenumber (ω) is used along with frequency (ν) since they both are linearly proportional to photon energy (E). The following equations describe these relationships.[21]

The relation between wavelength and its frequency: $\lambda = \frac{c}{\nu}$; c = speed of light

The relation between frequency and photon energy: $\nu = \frac{\Delta E}{h}$; h = Planck constant

The relation between wavelength and wavenumber: $\omega = \frac{\nu}{c} = \frac{1}{\lambda}$

The wavenumber (ω) is defined as the number of wavelengths (λ) per unit distance and it is commonly represented in cm^{-1}.

In the case of inelastic scattering, when light interacts with molecules that are polarizable, the energy from the light distorts valence electrons, exciting the molecule to a fleeting state (known as the virtual state) whose energy is determined by the frequency of the light source used. During the scattering process, nuclear motion is induced and energy is transferred from the incident light to the molecule. The difference between the incident energy and the energy transferred to the molecule is the scattered light energy. This type of scattering, where the scattered energy frequency is less than that of the exciting energy is known as the Stokes scattering. The opposite scenario, where the scattered energy frequency is greater than that of the

excitation energy, is known as anti-Stokes scattering. The difference in energy from the incident light is obtained by subtracting the energy of the measured scattered light from that of the known energy of the incident light and this is known as the Raman scattering energy shift. These phenomena are illustrated in Figure 2, which was reproduced and modified from the Habteyes group overview presentation slides.

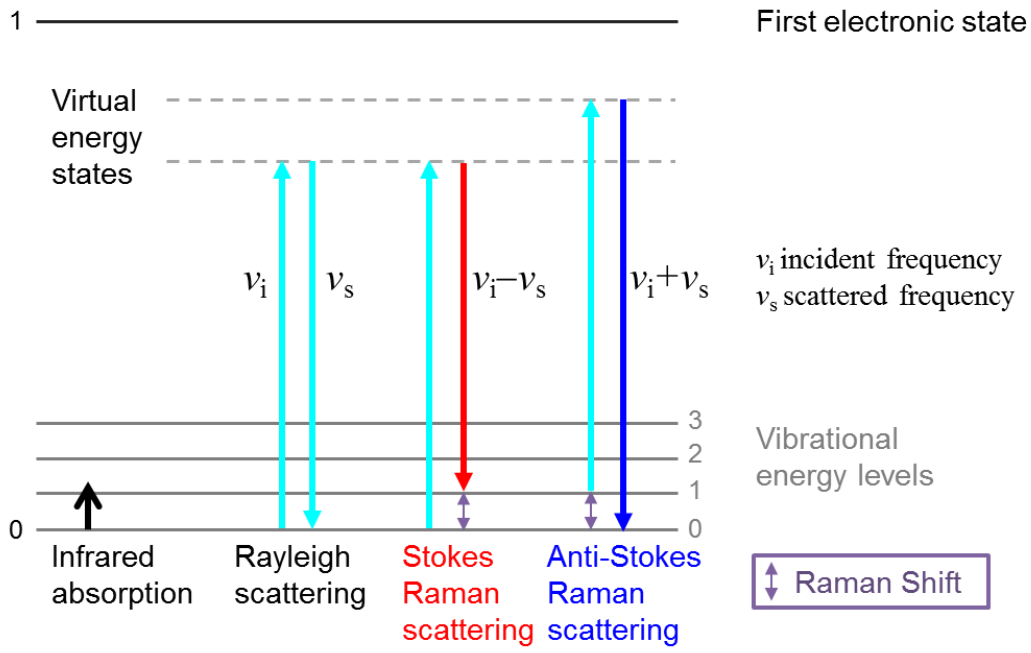

Figure 2: Simplified Jablonski Diagram Illustrating Rayleigh and Raman Scattering

Spectra obtained from Raman spectroscopy experiments are unique to the molecules under investigation. The collection of the Raman shifts, or bands, which make up the spectra are a function of the size of the atoms, the arrangement of the atoms in the molecule, and the chemical bond strength, which influence molecular vibrations. Therefore, even subtle modifications to the molecule will be reflected in the spectra. Although primarily advantageous as an analytical technique, the Raman scattering effect is remarkably weak and produces low signal intensity spectra making it a suboptimal analytical technique for the identification of underground fluid tracer

molecules, particularly as they decrease in concentration over time. To overcome this limitation, a relatively modern Raman technique known as Surface-Enhanced Raman Spectroscopy (SERS) provides significant signal enhancement while maintaining the advantages of a traditional Raman spectroscopic analysis such as being a non-destructive quick analytical technique and only requiring a small amount of sample, for example. Average Raman signal enhancements due to SERS are estimated to range from 10^4 to 10^6 and enhancements as high as 10^{12} have been reported.[21-23] Due to this large increase in the magnitude of normally weak signals, it is possible that SERS can be a valuable tool as a reliable and high-resolution detection method for small quantities of target molecules and may even work at the single molecule level.[24] A new advantage to report is that there has been recent development of cost-effective, portable handheld SERS spectrometers that can now be used in the field adding further appeal to this technique due to the relevancy to the application of subterranean fluid flow tracking.[8]

Surface-Enhanced Raman Spectroscopy, referred to as SERS from this point forward, is a technique whose source of signal enhancement is still under considerable debate in the scientific community. The most widely accepted mechanism involves electromagnetic enhancement through the excitation of localized surface plasmon resonances (LSPR).[16,23] LSPRs can be described as the type of constructive resonances that result from oscillations of a metal's electrons that are induced upon exposure to an incident electric field, such as that of a laser.[25] The collection of these electron oscillations, which occur on the surface of certain metals, are known as

plasmons and are characterized by charge separation on the surface of the metal.[20] Metals exhibiting this phenomena are known as plasmonic materials and they are often metal nanostructures such as Silver (Ag), Gold (Au), or Copper (Cu) spheres or rods.[26,27] Although these metal nanostructures may be the current standard, SERS is not limited to these materials and advances are currently being made in the development of new SERS substrates.[28] The basic concept is that if an analyte is placed on or very close to these metal nanostructures or SERS substrates, the plasmons will significantly amplify the Raman signal intensity.

The mechanism by which the SERS enhancement occurs is initiated by amplifying the electromagnetic field on the surface of the metal nanostructure. This is accomplished by excitation with a laser. This amplified electromagnetic field (LSPR) then couples with the incident laser photons which sharply enhance the amplitude of the electromagnetic field at the surface. The analyte sample on the surface experiences a very strong localized electric field, increasing the Raman scattering of the analyte. Therefore the overall SERS intensity is achieved when the wavelength of the incoming energy is in resonance with the LSPR peak of the metallic nanonstructure.[22] This proposed mechanism describes the scenario of SERS enhancement due to the incident excitation wavelengths that match the plasmon resonance but does not take into account the molecule-metal system together.[24] Taking into account the molecular contribution, it is expected that the SERS detection sensitivity can significantly increase if the excitation wavelength overlaps not only with the plasmon resonance but with the molecular resonance as well.[24,29]

This research will investigate salen-type ligands. The primary objective is to answer if, qualitatively, the salen-type ligands are effective candidates for subterranean fluid flow tracers and if SERS is a useful analytical technique to detect them above ground. The secondary objective is to answer if, quantitatively, SERS can be a useful analytical technique to identify the salen-type ligands as their concentration in underground reservoirs decrease over time. An exploratory SERS investigation into the aqueous ligand based metal-ligand complexes will provide insight into the effect of complexation on the application of this work. The investigative analysis into determining the viability of a salen-type ligands based monitoring system that can be used to track fluid flows underground and identified with SERS is now presented follows.

2. Experimental

2.1. Synthesis

2.1.1. Ligands

Following established routes, a family of salen derivatives was synthesized, each one ranging in hydrocarbon or aqueous solubility[9]. The complete list of salen-type ligands made to date is found in Table 16 and Table 17, however this work is primarily focused on three aqueous-soluble ligands (RAK6-8). Two hydrocarbon-soluble ligands (RAK0-1) will be briefly looked at due to their solubility properties. The reaction is an intermolecular condensation between an aldehyde and a primary amine forming an imine derivative, also known as a Schiff base (compounds having the general structure R2C=NR). The amine forms the resulting imine bridging group for the structure. All chemicals were used as received from Sigma Aldrich and Alfa Aesar without further purification. All ligands made were characterized by all or some of the following analytical techniques: proton nuclear magnetic resonance (^{1}H-NMR), Elemental Analysis, Single crystal X-ray crystallography not included in this manuscript. Fourier transform-infrared (FTIR) data was provided and summarized in this report, however the spectra was not made available. With the exception of the Raman and UV-Vis spectroscopic analysis, which was carried out by the author, all analytical characterization was carried out by Kemp and Boyle research group members.

Unless otherwise specified, all syntheses were carried out on a double-manifold Schlenk vacuum line and in a glove box, each under an atmosphere of argon.

2.1.1.1. Hydrocarbon Soluble Ligands

Initial exploratory work focused on hydrocarbon soluble ligands. In particular two ligands, RAK0 and RAK1 identified in Table 1, were of interest for their potential application to natural gas and oil subterranean well monitoring. Preliminary work with these ligands established a baseline understanding of the chemistry involved and helped shift the focus to investigate water soluble ligands, covered in the next section.

Identification	Chemical Abbreviation	Bridging group	Aldehyde derivative/attached group
RAK0	H_2Salo-Bu^t	Ethylene	3,5-di-*tert*-butyl
RAK1	H_2SaloPh-Bu^t	Phenylene	3,5-di-*tert*-butyl

Table 1: Nomenclature Summary for Hydrocarbon Soluble Ligands

Syntheses of the following two ligands were performed by the author.

The first ligand prepared was N,N'-bis-(3,5-di-*tert*-butylsalicylidene)-1,2-ethylenediimine, referred to in the literature as H_2Salo-Bu^t and internally referred to as RAK0 amongst the Kemp and Habteyes research groups. Synthesis of RAK0 was prepared by refluxing 3,5-di-*tert*-butylsalicylaldehyde with ethylenediamine while undergoing continuous stirring in a 2:1 molar ratio using methanol as a solvent. The reaction was carried out for three hours

at a temperature of 65°C and at the end of the reaction, the ligand was obtained after filtration and dried *in vacuo* in the form of a light yellow powder.

The second ligand prepared was N,N'-bis-(3,5-di-*tert*-butylsalicylidene)-phenylenediimine likewise referred to as H_2SaloPh-Bu^t in the literature and internally as RAK1 amongst the research group members. Synthesis of RAK1 was prepared by refluxing 3,5-di-*tert*-butylsalicyladlehyde with o-phenylenediamine while undergoing continuous stirring in a 2:1 molar ratio using methanol as a solvent. The reaction was carried out for seventeen hours at a temperature of 65°C and at the end of the reaction, the ligand was obtained after filtration and dried *in vacuo* in the form of a bright yellow powder.

The conventional reaction schemes for these ligands are depicted in Figure 3, not shown to reflect stoichiometric quantities.

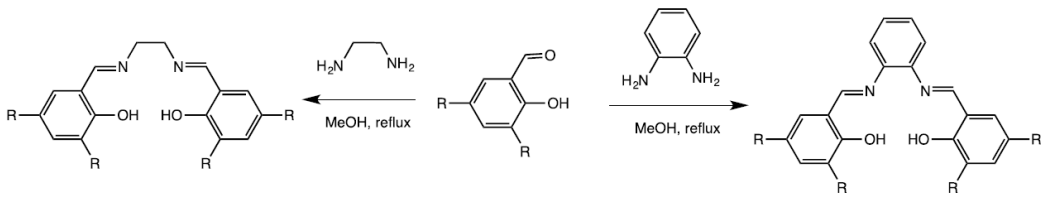

Figure 3: Reaction Scheme for Synthesis of Hydrocarbon Soluble Ligands

2.1.1.2. Aqueous Soluble Ligands

The following ligands were designed and synthesized with ionic components to increase the solubility in aqueous solutions, following on established routes, with slight modification.[12] These ligands, RAK6-8, included a polar backbone and an ionic attached group to the aldehyde and are studied for their potential application to subterranean geothermal well monitoring. Table 2 contains a summary of the ligands made and their nomenclature.

Identification	Chemical Abbreviation	Bridging Group	Aldehyde derivative/attached group
RAK6	H_2Salo-P$Ph_3[Cl^-]_2$	Ethylene	Methyl (triphenylphosphonium) chloride
RAK7	H_2SaloPh-P$Ph_3[Cl^-]_2$	Phenylene	Methyl (triphenylphosphonium) chloride
RAK8	H_2SaloPy-P$Ph_3[Cl^-]_2$	Pyridine 2,6 diamine	Methyl (triphenylphosphonium) chloride

Table 2: Nomenclature Summary for Aqueous Soluble Ligands

The precursors for these ligands were prepared by Orion Staples and the ligands were prepared by Kevin Wyss, both from the Kemp research group[30].

The ionic portion on the aldehyde was prepared as follows:
Synthesis of the ionic aldehyde, 5-methyl(triphenylphosphoniumchloride)-2-hydroxybenzaldehyde, was prepared by adding 5-(Chloromethyl)-2-hydroxybenzaldehyde to a round bottom flask containing acetonitrile as the medium-polarity solvent as it is both miscible with water and a range of organic solvents. To the reaction mixture, triphenylphosphine was added and

allowed to mix while undergoing continuous stirring. The reaction was carried out for twenty-four hours at a temperature of 82 °C. The aldehyde precursor was obtained after filtration and dried *in vacuo* in the form of an off-white powder.[30]

Refer to the reaction scheme in Figure 4 for an illustration of the precursor synthesis.

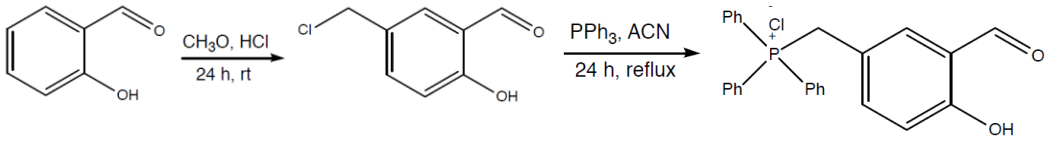

Figure 4: Reaction Scheme for Synthesis of the Ionic Aldehyde Precursor

The synthesis of the water soluble ligands then proceeded as follows, with the only difference being the amine used. The reaction schemes for these ligands are provided in Figure 5.

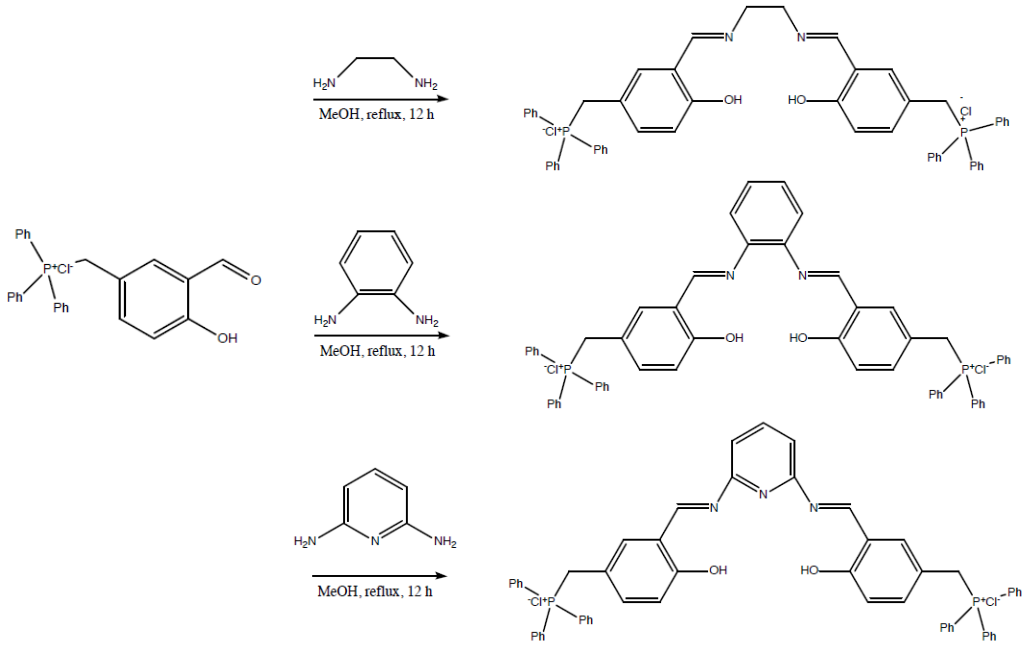

Figure 5: Reaction Schemes for Synthesis of Aqueous Soluble Ligands

2.1.2. Metal-Ligand Complexes

Water soluble ligands, RAK6-8, were chosen for this applied research study and as such were complexed to metal. Ligands RAK 6-8 were successfully complexed to Magnesium by Kevin Wyss of the Kemp group.

The water soluble ligands, RAK6-8, were reacted with Mg metal ions to prepare the final metal-ligand (M-L) complexes. Upon complexation, these dianionic ligands become deprotonated and can be prepared by classical methods such as ion exchange, eliminations, or protonation reactions. Complexation of these ligands was carried out in a glove box with an atmosphere of argon.

Refer to Table 3 for a summary of the ML complexes and nomenclature.

Identification	Chemical Abbreviation	Bridging Group	Aldehyde derivative/attached group
MgRAK6	MgSalo-$PPh_3[Cl^-]_2$	Ethylene	Methyl (triphenylphosphonium) chloride
MgRAK7	MgSaloPh-$PPh_3[Cl^-]_2$	Phenylene	Methyl (triphenylphosphonium) chloride
MgRAK8	MgSaloPy-$PPh_3[Cl^-]_2$	Pyridine 2,6 diamine	Methyl (triphenylphosphonium) chloride

Table 3: Nomenclature Summary for Metal Coordinated Aqueous Soluble Complexes

2.2. Proppant Loading and Surface Coating

Proppant loading was carried out by Orion Staples from the Kemp research group. Uncoated, ceramic porous proppants under the name 20/40 CarboUltraLite were provided by Carbo Ceramics, Inc. and contained approximately 0.112 mL/g of interconnected pore volume available for ML complex loading.[31] It was determined that a loading target of 90% ML complex in the available pore volume would be optimal to mitigate surface deposition. This translated to the desired weight loading target between 2 and 6 wt. % ML Complex in proppant.[31]

The experimental procedure for loading 2-6 wt. % MgRAK6-8 Complexes into the proppant was as follows:

To an empty pre-weighed vial, a measured amount of metal ligand complex was added to 15 mL of methanol. To a second empty pre-weighed vial, 15.000 g of proppant was added. For each loading, 1.5 mL of metal ligand solution was added

dropwise to the vial containing proppant, shaken to ensure complex was taken up via capillary forces, and mixed at a temperature of 150 °C for two hours *in vacuo* to remove the solvent. The process was repeated until the desired target wt. % range was achieved for each ML Complex.

MgRAK6

0.540 g MgRAK6 was deposited into 15.000 g proppant via the previously described method. This loading achieved 3.60 wt. % MgSalo-$PPh_3[Cl^-]_2$ in proppant.

MgRAK7

0.744 g MgRAK7 was deposited into 15.000 g free proppant via the previously described method. This loading achieved 4.96 wt. % MgSaloPh-$PPh_3[Cl^-]_2$ in proppant.

MgRAK8

0.861 g was deposited into 15.000 g free proppant via the previously described method. This loading achieved 5.74 wt. % MgSaloPy-$PPh_3[Cl^-]_2$ in proppant.

Loaded proppants were mailed to Carbo Ceramics, Inc. where a portion of the loaded proppants can then be coated with an epoxy polymer to help “time release” the M-L complex from the proppant during use. The technology completing this is proprietary, therefore the procedure is not available to present nor is it too relevant as the initial studies focused on uncoated proppants.

2.3. Elution Studies

Elution studies were carried out to simulate fluid flow in a hydraulically fractured zone containing proppants.

Carbo Ceramics, Inc. performed elution testing on the non-polymer coated proppant packages. Again, only the non-polymer coated elution studies will be investigated however the elution testing procedure is the same in either case.

Representative fluids such as oil/gas reservoir fluids or Isopar G (hydrocarbon) and sea water solution (aqueous) were pumped through known volumes of loaded proppant packages in a plastic syringe. The fluid volume required to fill the space between the proppant particles in the packed syringe is considered one pore volume, and the laboratory testing included hundreds of pore volumes. After passing over the proppant package, where the loaded M-L complex elutes into the fluid, the fluid samples were separated into fractions for evaluation using inductively coupled plasma mass spectrometry (ICP-MS) analysis (performed at Carbo Ceramics, Inc.) and SERS (performed at the Habteyes laboratory). A photo of the automated laboratory elution testing setup using seawater is shown in Figure 6. A cartridge pump sends the fluid from right (the seawater reservoir) to left (the proppant packed syringes) and into the fractionated receiver. A rubber septa is used to create a seal on top of the proppant pack which created pressure to force the fluid into the tubing and to the collection test tubes in the fraction collector. Finally, the concentrations of the metal complexes in the samples were measured by the ICP-MS.

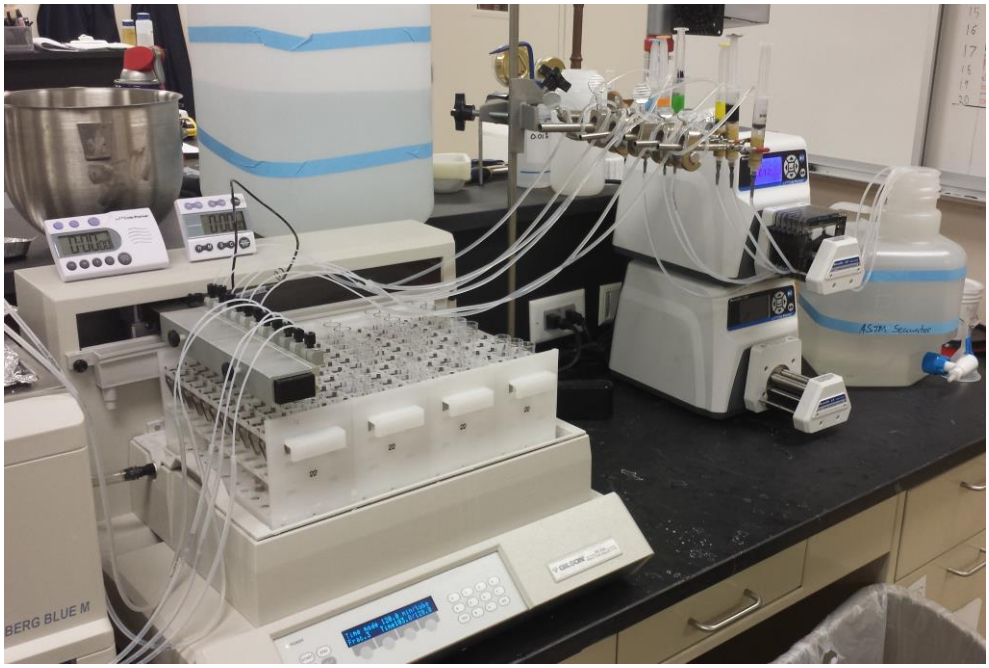

Figure 6: Elution Setup at Carbo Ceramics, Inc.

MgRAK6 Elution profile

3.60 wt. % MgRAK6 loaded proppant, uncoated, was packed into an elution syringe. ASTM Seawater (657 mg/mL Mg) was pushed through the syringe at a flow rate of (0.1188 mL/min) for 111.5 hours. ICP-MS measurements taken throughout the elution process were taken from samples collected at specific intervals and sent to the Kemp and Habteyes labs for further analysis. Known Mg concentration from the ASTM seawater was subtracted from the measurements.

MgRAK7 Elution profile

4.96 wt. % MgRAK6 loaded proppant, uncoated, was packed into an elution syringe. ASTM Seawater (657 mg/mL Mg) was pushed through the syringe at a flow rate of

(0.1092 mL/min) for 103.5 hours. ICP-MS measurements taken throughout the elution process were taken from samples collected at specific intervals and sent to the Kemp and Habteyes labs for further analysis. Known Mg concentration from the ASTM seawater was subtracted from the measurements.

MgRAK8 Elution profile

5.74 wt. % MgRAK6 loaded proppant, uncoated, was packed into an elution syringe. ASTM Seawater (657 mg/mL Mg) was pushed through the syringe at a flow rate of (0.1033 mL/min) for 111.5 hours. ICP-MS measurements taken throughout the elution process were taken from samples collected at specific intervals and sent to the Kemp and Habteyes labs for further analysis. Known Mg concentration from the ASTM seawater was subtracted from the measurements.

2.4. Ultraviolet-Visible Spectroscopy

UV-Vis spectroscopy was performed by the author for hydrocarbon soluble ligands, RAK0-1, and for aqueous-soluble ligands, RAK6-8 and their complexes. Ethanol was the solvent chosen for RAK0-1 and water was chosen for RAK6-8 and MgRAK6-8. Table 4 contains a list of the concentrations of the stock solutions.

Samples were prepared in 1000 μL quartz cuvettes. Several test runs were completed to determine the amount of solutes to use in the solvents. This was determined by adjusting the amount of solute until the absorbance bands were within a desired range and not saturating the detector. For all UV-Vis samples, the amount of each sample

used in solution ranged from 2-5 drops into the cuvette. Care was taken to ensure no air bubbles were inside the cell and that the outsides of the cell were clean and free. Cuvettes were wiped clean prior to placing them in the spectrometer for analysis.

UV-Vis absorption data was obtained on a Shimadzu UV-2450 Ultraviolet-Visible spectrophotometer.

2.5. Surface-Enhanced Raman Spectroscopy

SERS Analysis was performed in the Habteyes laboratory. Two lasers are available as potential excitation sources for Raman spectroscopy experiments, a 633 nm laser and a 532 nm laser. As stated earlier, overlapping the excitation source with the electronic transition band of the molecule leads to a significant increase in signal known as resonance Raman (rR) spectroscopy but it was determined that the molecules absorbed in the near UV region. Therefore the determination of which laser to use was based on overlapping the laser resonance with the plasmonic materials. After a survey of the available plasmonic metal nanostructures, colloidal gold nanorods that absorb at 700 nm (AuNR 700), were selected for this analysis. For AuNR 700, plasmon peaks are observed in the visible region of 700 nm and can therefore overlap with excitation frequency of the 633 nm laser, creating a strong enhancement. Figure 7 shows the spectral overlap of AuNR 700 with the 633 nm laser used as the excitation source for all SERS in this experiment.

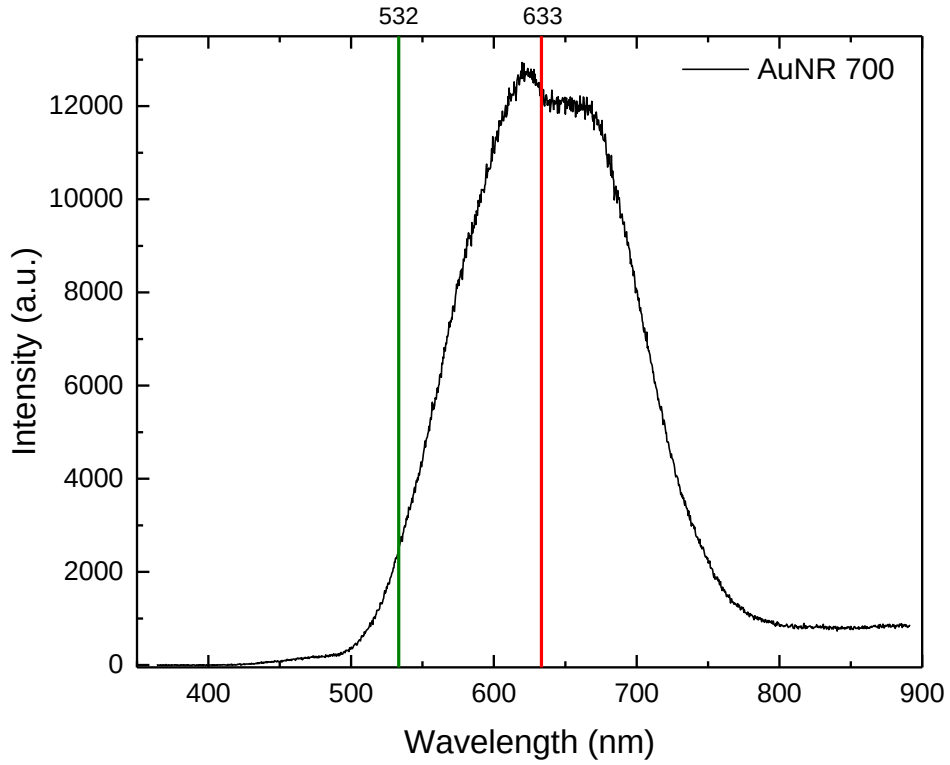

Figure 7: Spectral Overlap of the 633 nm Laser Line with the Plasmon Resonance

2.5.1. Sample Preparation

SERS samples for this study were prepared as three layer structures where the analyte was deposited on a support coated with metal nanoparticles.

The first step in the sample preparation process is the cleaning of the support, which is an oxide coated silicon wafer. The wafer underwent a series of sonication intervals while submerged in a solvent. In this case, the wafer was first submerged in acetone and sonicated for 5 minutes, rinsed with and submerged with Isopropanol and sonicated for 5 minutes, rinsed with and submerged in DI ultrapure water with 5 minutes sonication. The support is then carefully removed from the beaker, dried with N_2 gas and placed in a UV ozone cleaner, Novascan

PSD Pro Series Digital UV Ozone System, for approximately five minutes where remaining contaminants were removed by UV radiation. In addition to surface cleansing, this process also improves the adhesive property of the support.

Concurrently, the nanoparticles are prepared for deposition onto the support. An aqueous solution of gold nanorods (AuNRs) with cetyltrimethlammonium bromide (CTAB) obtained from Nanopartz, Inc. undergo an extraction process aimed at removing CTABs strongly bound to the AuNRs. CTABs function to stabilize the gold nanorods but are removed so as not to introduce an unwanted species in the sample. To efficiently remove the stabilizing surfactants without hampering the stability of the Au nanorods, the AuNR solution undergoes two rounds of centrifugation (5000 rpm for 5 minutes), each time carefully removing the supernatant following the centrifugation. The AuNRs are then re-suspended in DI ultrapure water and flash sonicated to ensure dispersion. The suspension was then deposited on the clean support, the oxide coated silicon wafer. This was accomplished by drop casting the nanoparticle dispersion on to the clean oxide coated silicon wafer and allowing it to naturally evaporate, a process which can take up to an hour. During the AuNRs evaporation process the nanoparticles are drawn together by capillary forces resulting in a layer of nanospheres uniformly adhered onto the support. Visual inspection is used to confirm the evaporation has occurred and then the analyte can be placed on the sample. Refer to Table 4 for the concentrations of ligands prepared. Concentrations were not available for the metal ligand complexes but for all samples, approximately 10 μL were drop

casted onto the AuNR-SiO2 substrate and allowed to evaporate. The prepared and finalized sample are shown in Figure 8. Once evaporation has taken place, the samples can be mounted on the microscope in preparation for spectroscopic analysis.

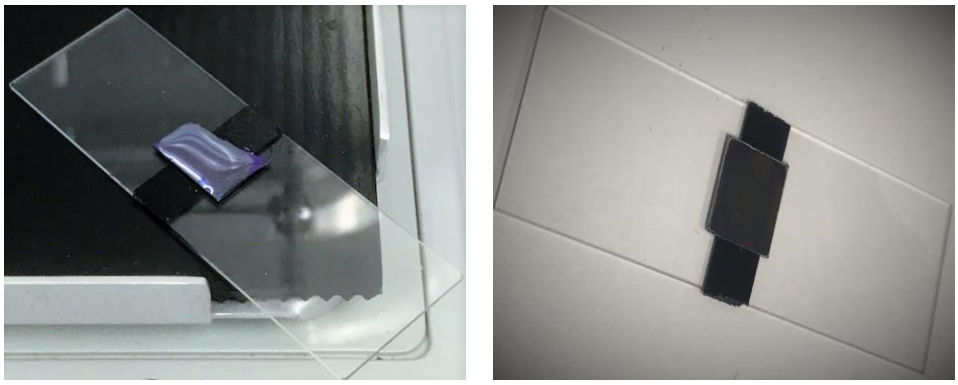

Figure 8: Photographs of Mounted Samples;left: Drop Cast Sample, right: Dried Sample

Solutions of Ligands in Solvent were prepared as follows:

Ligand	Molecular Weight (g/mol)	Amount Solute (g)	Amount Solution (mL)	Molarity (M)	PPM
RAK0	492.8	.0049	10.19 (EtOH)	.0007 (10^{-4})	379
RAK1	540.8	.0052	10.18 (EtOH)	.0008 (10^{-4})	406
RAK6	889.8	.0150	17.49 (H_2O)	.0009 (10^{-4})	858
RAK7	937.9	.0176	17.03 (H_2O)	.0011 (10^{-3})	1034
RAK8	938.9	.0165	17.57 (H_2O)	.0010 (10^{-3})	939

Table 4: Concentrations of Ligands in Solution

2.5.2. Spectroscopic Characterization

Figure 9 illustrates the general SERS analysis setup in the Habteyes lab. A detailed explanation follows.

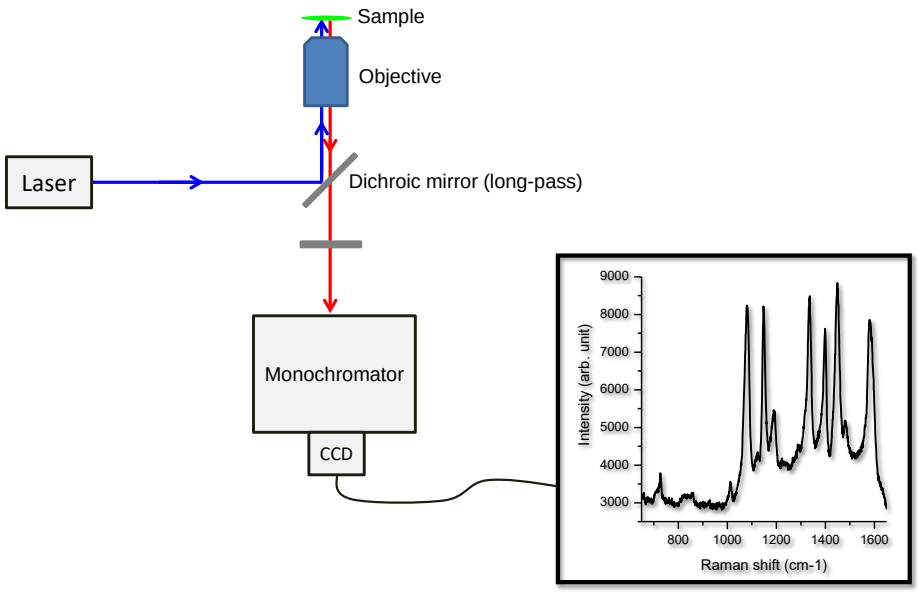

Figure 9: Schematic of the SERS Experimental Setup

2.5.2.1. Optical Setup

The following is a detailed description of the arrangement of optical components depicted in Figure 10. A 633 nm laser beam is directed toward an isolator, which is an optical component that constrains the transmission of light in only one direction to prevent unwanted feedback into the laser cavity. The laser beam then passes through a beam expander. Mirrors, common optical elements, are used on the bench to help direct light. The band pass filter then passes a narrow frequency (632.8 – 633.2 nm) through while attenuating frequencies outside this range. The band pass filter also removes plasma emission lines, improving the spectra. Next a set of neutral density filters, or optical attenuators, are used to reduce the intensity of the beam to achieve the best signal during an experiment. Filters can be adjusted to reduce power and avoid saturation into the spectrometer. Apertures #1 (and #2) function to narrow or widen the collimated laser beam which help fine-tune

the focus. As the laser prepares to enter the microscope it passes through a specialized dichroic mirror that selectively separates the light. This mirror is highly reflective below the 633 nm wavelength, allowing only wavelengths 633 nm and shorter to travel forward and toward the sample. Additional mirrors help guide this excitation laser beam toward the sample, which is mounted on a substrate. At this point, the SERS measurement begins. Scattered light from the sample is collected from a mirror (not shown) positioned at an angle inside the microscope. The scattered light, which is less intense than the incident light, passes through the aperture and encounters the specialized dichroic mirror which only passes light greater than the 633 nm wavelength. This lower energy, longer wavelength light is the inelastic, Raman scattering that will be measured. It should be mentioned that if there is any feedback from wavelengths below 633 nm, it will be reflected away and not allowed to pass through. Due to the significant intensity decrease, this is negligible amount of light. This scattered light is then directed toward the spectrometer for measurement by first passing through a long pass filter, which selectively passes only the longer wavelengths and blocks the shorter ones. Finally, the light passes through a focusing lens and into the spectrometer which measures and records the intensity of the light as a function of its wavelength.

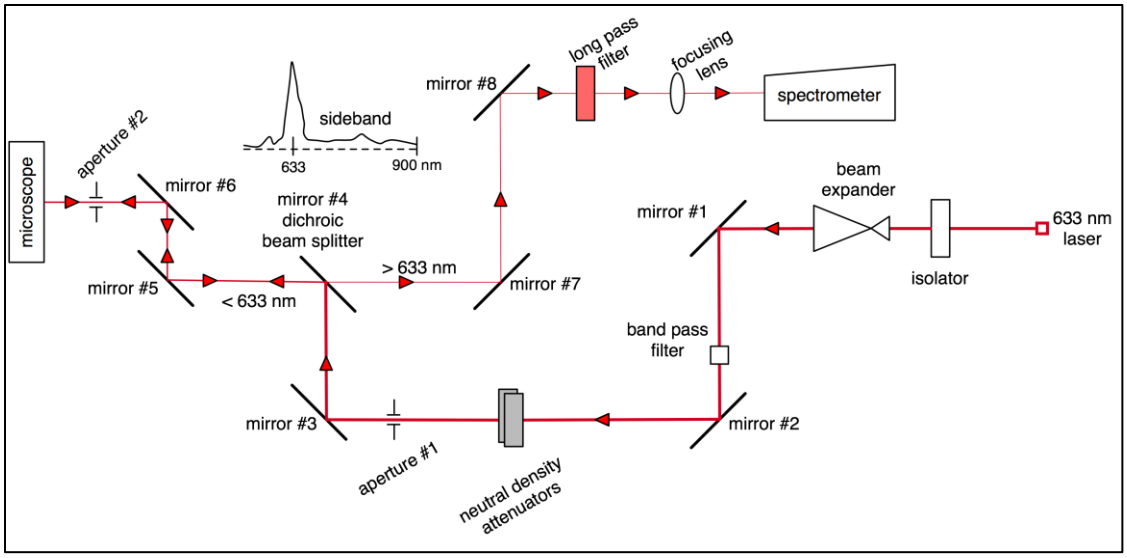

Figure 10: Detailed Depiction of the Optical Component Arrangement for SERS Analysis

2.5.2.2. SERS Measurement

The excitation source used for all of the molecules studied was a 633 nm Helium-neon (HeNe) laser. As described earlier, the laser beam travelled through various optical components and reflected off of multiple mirrors that directed the light to an inverted Olympus GX51 microscope equipped with a dark-field objective (0.9NA, 100x) where optical characterization was performed. Prepared SERS samples were affixed on a glass slide and mounted on a stage that oriented the sample facing the front lens of the objective on the microscope that can dually illuminate the sample with white light and excite the sample with the laser light. Figure 11 portrays a detailed view of this setup. Scattered light collected from the sample passes back through the objective. More than 90% of the light collected from the sample through the objective was directed to the spectrometer (IsoPlane Spectrograph, Princeton Instruments) and a thermoelectrically cooled (-75°C) and back-illuminated

deep depletion CCD camera. The remaining light collected from the sample was directed to a camera attached to the microscope that provided imaging of scattered light from the sample using bright and dark field. All measurements were carried out using an exposure ranging from 5000 to 10000 ms in the range 300-1700 cm^{-1}.

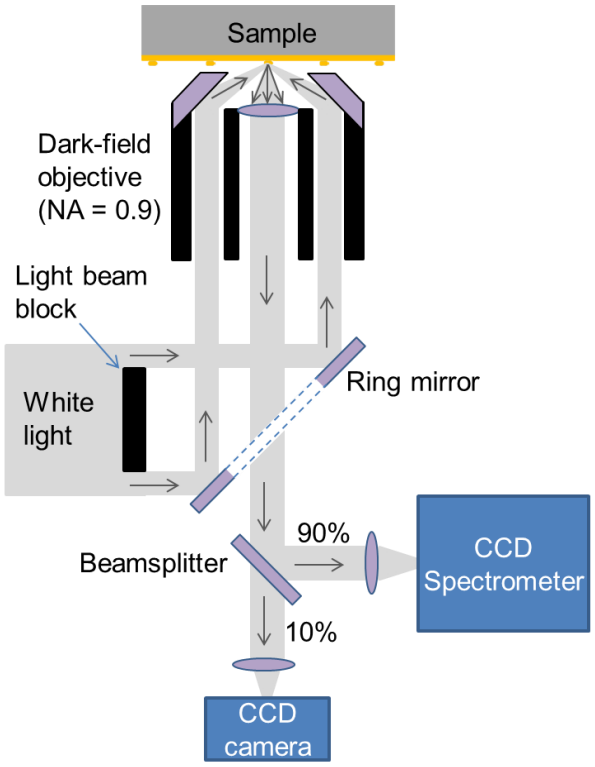

Figure 11: Schematic Showing a Detailed View of the Microscope

This setup allows for the selectivity of the desired location on the sample from which to measure the Raman scattering. This is accomplished by simply switching the excitation source from monochromatic laser light to white light and moving the sample stage using a controller to select the exact region from which to obtain spectra. Dark field images can also be obtained and directly compared to obtained spectra, real time, so as to maximize the technique and

obtain the spectra from specific areas of interest. A photograph of an active SERS analysis is depicted in Figure 12. To the left is a dark field image of RAK8 molecules adsorbed on the Silicon wafer with gold nanorods and to the right is an image of a spectra obtained from a selected spot on the prepared sample.

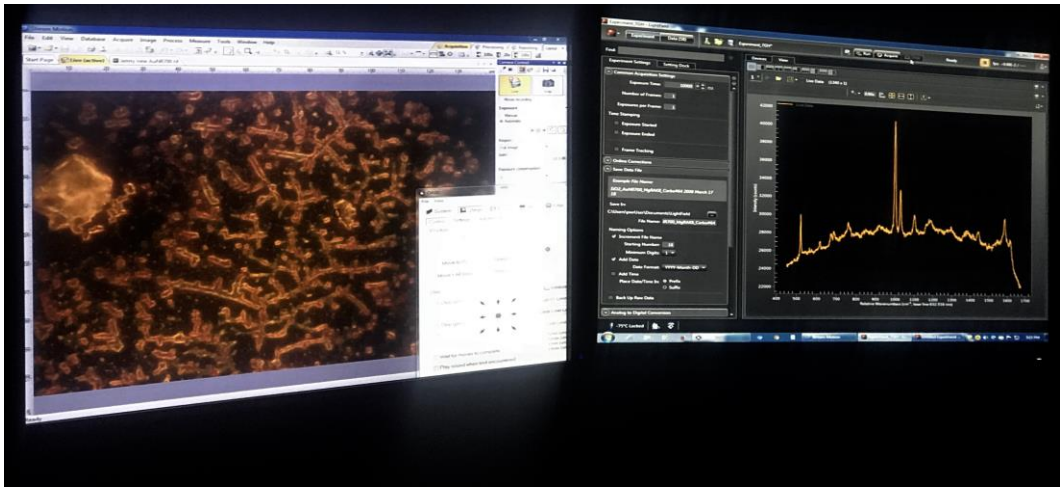

Figure 12: Photograph of an Active SERS Analysis

Olympus StreamMotion was the imaging analysis software used and Princeton Instruments LightField scientific imaging & spectroscopy software was used to acquire the spectra. All spectra were exported for data analysis using Origin graphing and analysis software. To convert the independent variable from wavelength (nm) to Raman shift (cm^{-1}), the following equation was used:

$$\Delta\nu = \left(\frac{1}{\lambda_0 nm} = \frac{1}{\lambda\, nm}\right)\left(\frac{10^7 nm}{cm}\right)$$

Commonly, the Raman scattering energy shift is expressed simply as cm^{-1} but technically it should be expressed as Δcm^{-1} since it is the shift or change in energy from the incident energy.[21] The data presented in this body of work will follow the standard convention and refer to the Raman shift as cm^{-1}.

3. Results and Analysis

3.1. Infrared Spectroscopy

Infrared spectroscopy was performed for all ligands and complexes in this study by members of the Kemp and Boyle groups using a Nicolet 6700 FTIR spectrometer using a KBr pellet press under Nitrogen atmosphere or with an iD7 ATR accessory mounted with a monolithic diamond crystal.[31] Refer to Table 5 and Table 6 for a summary of IR absorption peaks for key functional groups common to all the ligands under investigation.[30]

3.1.1. Hydrocarbon Soluble Ligands

Table 5 summarizes the Infrared (IR) absorption peaks for the two key vibrational modes in the hydrocarbon soluble ligands, RAK0 and RAK1. These vibrational modes were identified as key features as they are the binding sites to metals. A significant difference in the frequency of the peaks is observed due to their structural differences; RAK 0 contains an ethylene bridge and RAK1 contains a phenylene bridge in the ligand backbone. This difference can be attributed to the increased delocalization of electrons over the atoms in RAK1.

	IR Absorption peak (cm^{-1})	
Functional Group	RAK0	RAK1
C = N	1626	1615
C ─ O	1172	1169

Table 5: Summary of Key IR Absorption Peaks- Hydrocarbon Soluble Ligands

3.1.2. Aqueous Soluble Ligands and Mg-Ligand Complexes

The data in Table 6 describe the IR absorption peaks for the two key vibrational modes in the water soluble ligands, RAK6-8, and their corresponding Mg complexes. As in the hydrocarbon soluble ligands, these vibrational modes were identified as key features as they are the binding sites to metals. Differences in the frequency of the peaks between the ligands are observed due to their respective electronic environments influenced by the ethylenediamine, phenylenediamine, and pyridine backbones (addition of a heteroatom). The binding of the metal causes shifts in each of these key vibrational modes, confirming the formation of a complex.

	IR Absorption peak (cm^{-1})					
Functional Group	RAK6	MgRAK6	RAK7	MgRAK7	RAK8	MgRAK8
C = N	1631	1709	1610	1675	1618	1655
C ─ O	1160	1111	1189	1159	1108	1212

Table 6: Summary of Key IR Absorption Peaks- Aqueous Soluble Ligands and Their Mg-Complexes

3.2. Inductively Coupled Plasma Mass Spectrometry Analysis

Metal concentration, as determined by Inductively Coupled Plasma Mass Spectrometry **(**ICP-MS), sharply decreases within the first 20 hours of the elution process, as seen in Figure 13. This result indicates that uncoated proppants are not suitable for use in long-term subterranean fluid flow monitoring and that polymer coated proppants should elute Mg at a much lower rate.

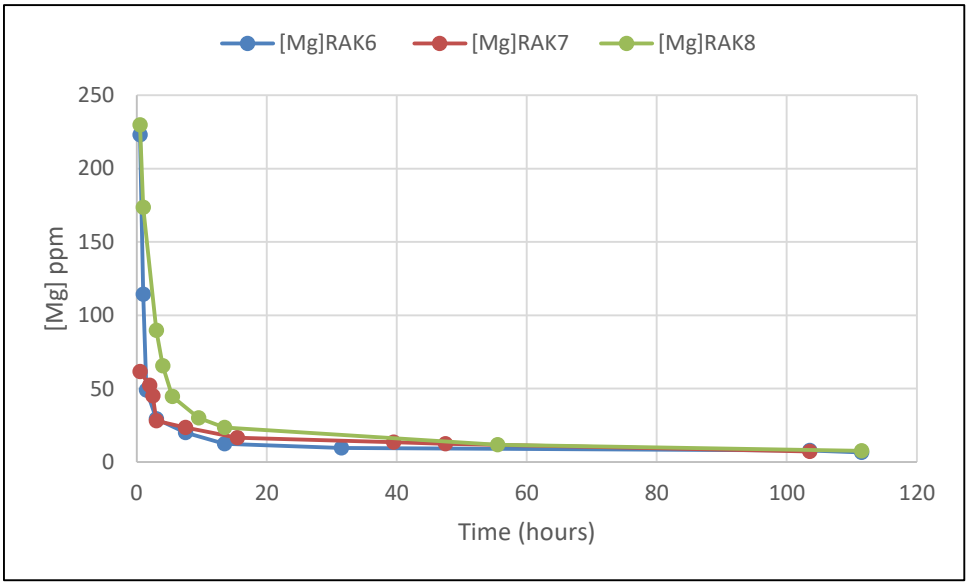

Figure 13: Carbo Ceramics, Inc. Elution Data for Metal Ligand Complexes in Uncoated Proppant

3.3. Ultraviolet-Visible Spectroscopy

Ultraviolet-visible spectroscopy was performed for all ligands and complexes by the author. Spectra and absorption maxima are summarized in the following sections.

3.3.1. Hydrocarbon Soluble Ligands

No significant absorption peaks were seen for the hydrocarbon soluble ligands beyond the range shown in Figure 14. These ligands absorb in the near UV range and differences seen can be attributed to the structural features of these ligands that affect electronic transitions. RAK0 and RAK1 absorb at expected wavelengths. RAK0 contains a saturated ethylene backbone so it is expected to absorb at a shorter wavelength and RAK1 exhibits absorption at the longer wavelength due to the presence of the phenylene backbone which increases the delocalization in the pi electrons. Table 7 summarizes the measured absorbance maxima of these ligands.

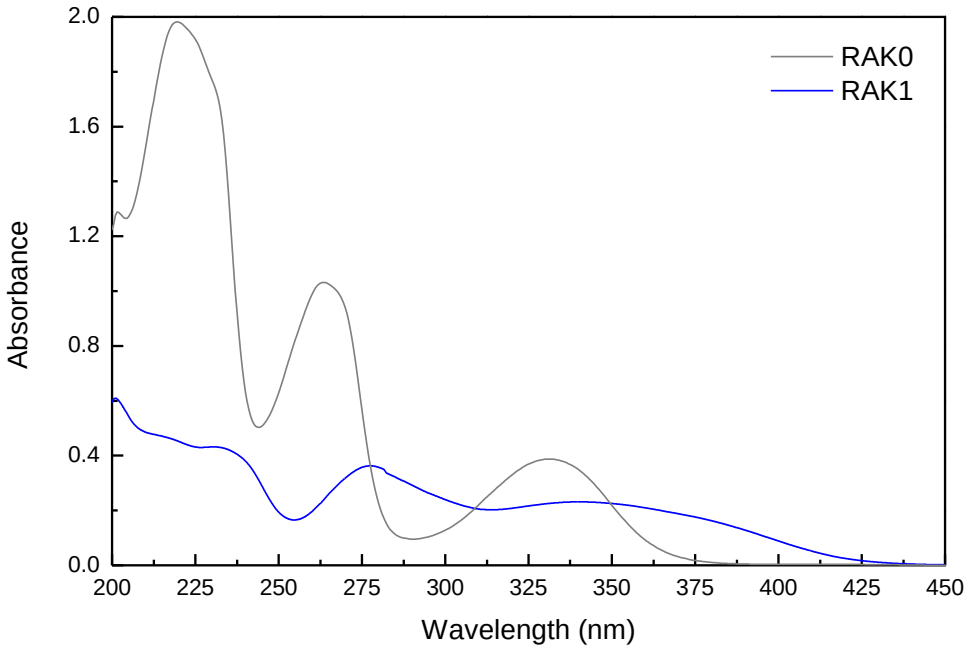

Figure 14: UV-Vis Absorption Data for Hydrocarbon Soluble Ligands

Ligand	Wavelength (nm)		
RAK0	220 (λ_{max})	264	331
RAK1	232 (λ_{max})	278	---

Table 7: Absorption Peaks for Hydrocarbon Soluble Ligands

3.3.2. Aqueous Soluble Ligands and Mg-Ligand Complexes

No significant absorption peaks were seen for the aqueous soluble ligands or their complexes beyond the range shown in Figure 15. However, there are subtle differences among the individual ligands, among their complexes, and among each other. The following plots have been created with an emphasis on the wavelength range where absorbance is greatest.

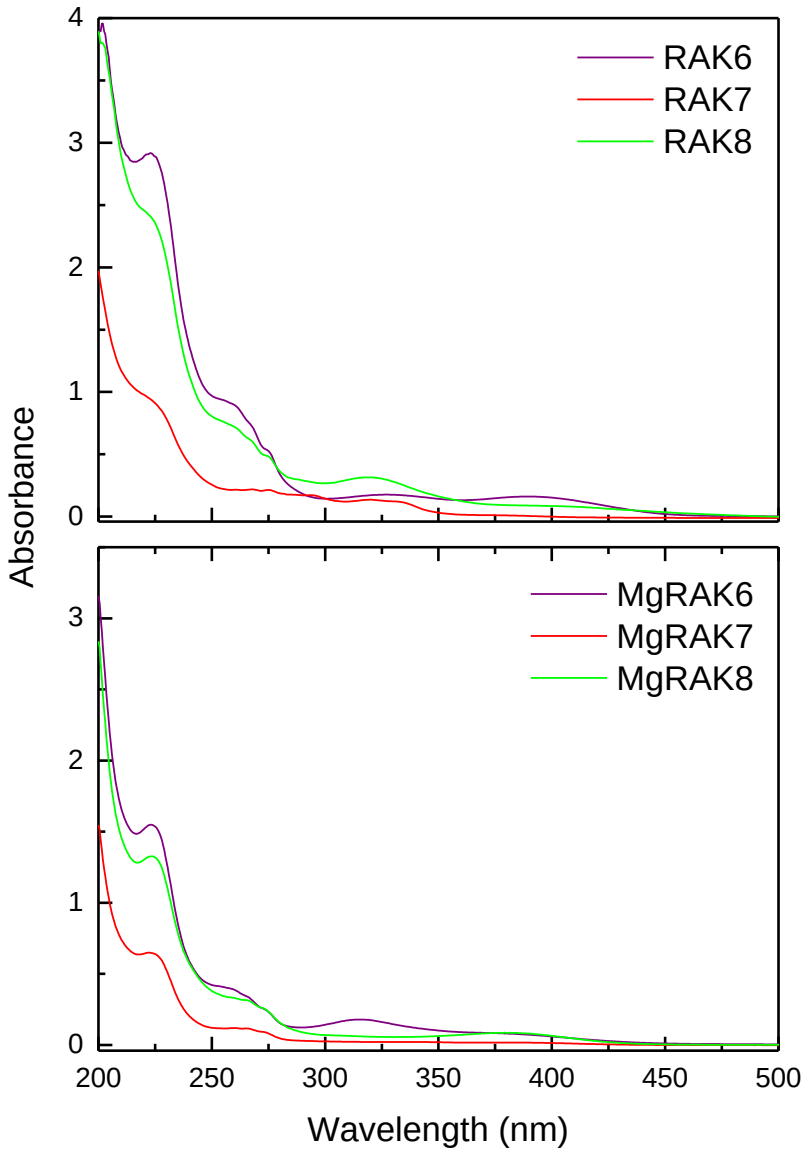

Figure 15: UV-Vis Absorption Spectra Comparison between Aqueous Soluble Ligands and Metal-Ligand Complexes

RAK6 ligand and its metal complex show a distinct difference in their absorption peaks due to the presence of the metal and the resulting effect on the electronic structure of the molecules. Figure 16 shows that compared to the ligand, the 327 nm band blueshifts to 315 nm and the 390 nm significantly decreases, possibly due to a charge transfer. The measured absorbance maxima of these ligands is summarized in Table 8.

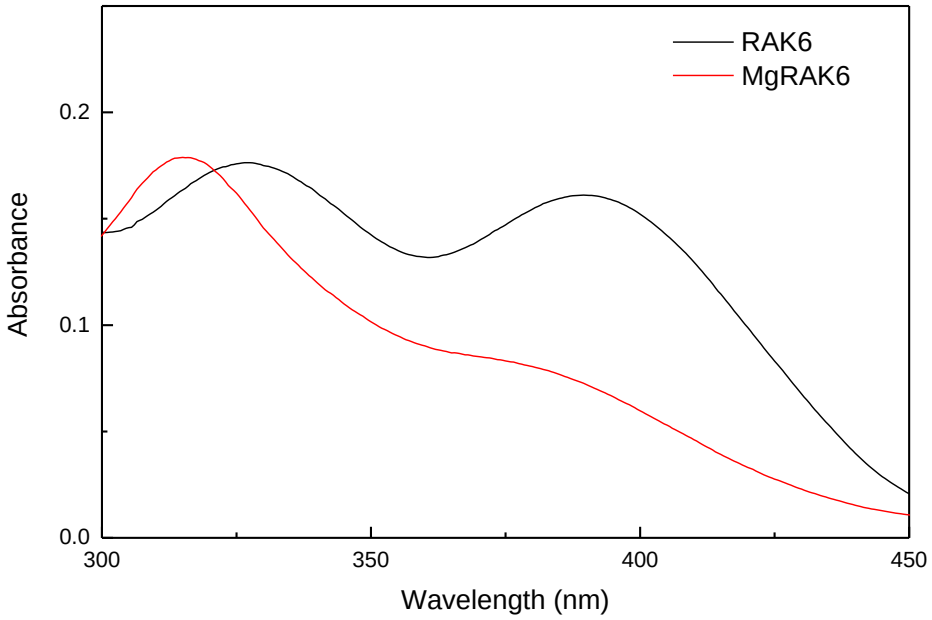

Figure 16: UV-Vis Absorption Spectra Comparison between RAK6 and MgRAK6

	Wavelength (nm)	
RAK6	327 (λ_{max})	390
MgRAK6	315 (λ_{max})	---

Table 8: Absorption Peaks for RAK6 and MgRAK6

Similar to the data shown in Figure 16, MgRAK7 ligand absorption spectrum is modified by the presence of the metal and the resulting effect on the electronic structure. The measured absorbance maxima of these ligands is summarized in Table 9.

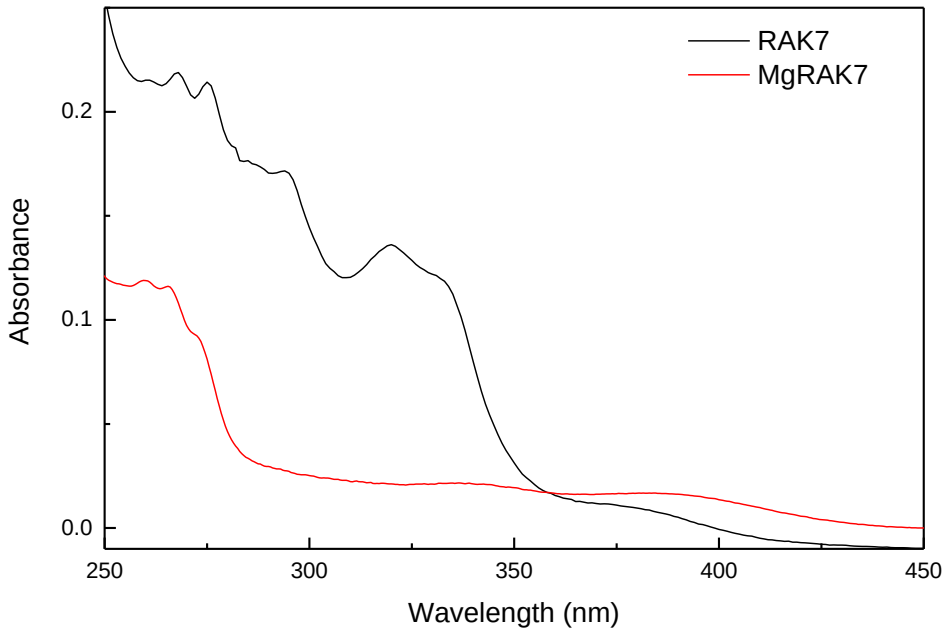

Figure 17: UV-Vis Absorption Spectra Comparison between RAK7 and MgRAK7

	Wavelength (nm)			
RAK7	268 (λ_{max})	275	294	320
MgRAK7	260 (λ_{max})	266	---	---

Table 9: Absorption Peaks for RAK7and MgRAK7

The data for RAK8 and its complex shows the redshift of the absorbance maxima for the complex indicating a possible stabilization due to the presence of the metal. The spectrum is shown in Figure 18 and the two absorbance peaks have been documented in Table 10.

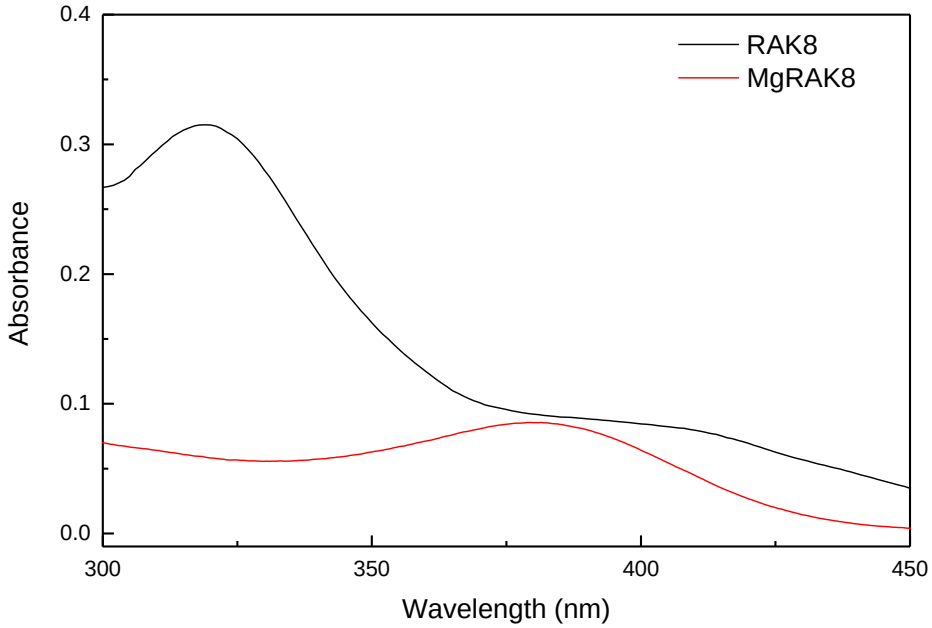

Figure 18: UV-Vis Absorption Spectra Comparison between RAK8 and MgRAK8

	Wavelength (nm)
RAK8	319 (λ_{max})
MgRAK8	380 (λ_{max})

Table 10: Absorption Peaks for RAK8 and MgRAK8

3.4. Surface-Enhanced Raman Spectroscopy

A note about the 520 cm^{-1} band observed in every SERS spectra. All SERS samples are prepared on thermal oxide coated Silicon wafers. A strong Raman peak at 520 cm^{-1} is observed from the Silicon wafers.

3.4.1. Hydrocarbon Soluble Ligands

SERS spectra for the hydrocarbon soluble ligands were not examined in detail as they are not the focus of this study and were not complexed with metals. The key functional groups for both of these ligands are the t-butyl group peaks seen in the 1200-1300 cm^{-1} range.[32] These peaks are not seen in the aqueous soluble ligands or their complexes, as expected.

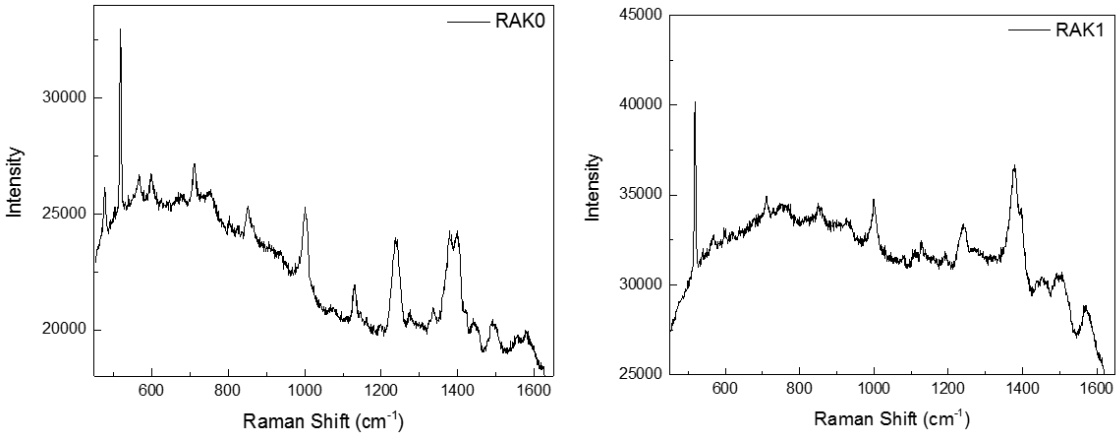

Figure 19: SERS Spectra Comparison between RAK0 and RAK1

3.4.2. Aqueous Soluble Ligands and Mg-Ligand Complexes

Figure 20-22 show the SERS spectra of the aqueous ligands and their Mg complexes. The data show the strongest ring breathing Raman modes at ~1000 cm^{-1} and ~1030 cm^{-1}. One reason that may explain this is due to the number of phenyl groups in these structures. The proposed assignments for these modes are found in Table 11-13. Other modes at higher and lower frequencies are relatively weak, in comparison. However, a slight difference in the spectra of RAK8 is found due to the additional Raman mode at ~1624 cm^{-1}. This mode is proposed to be C=N. The concentrations of the ligands and complexes used to prepare the samples for these SERS are as follows: RAK6 858 ppm, MgRAK6 223 ppm, RAK7 1034 ppm, MgRAK7 62 ppm, RAK8 939 ppm, and MgRAK8 230 ppm.

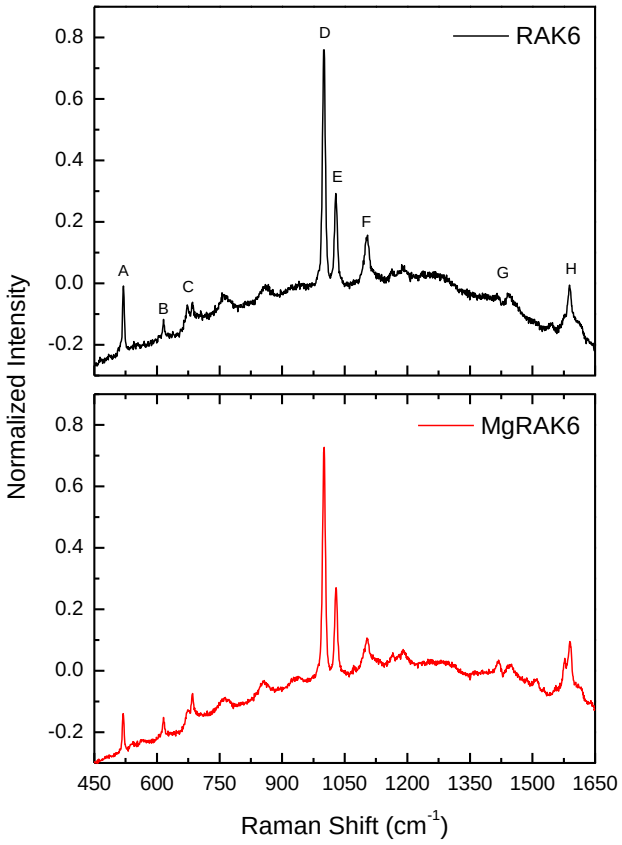

Figure 20: SERS Spectra Comparison between Ligand (RAK6) and Metal Ligand (MgRAK6) Complex

Peak Label	Ligand Raman Shift (cm^{-1})	Metal-Ligand Complex Raman Shift (cm^{-1})	Proposed Assignment
A	520	520	SiO_2 Substrate
B	616	616	
C	673	673	
	686	685	
D	1001	1001	Phenyl
E	1028	1029	Ring Breathing
F	1105	1105	
G	1415	1419	
	1440	1450	
		1577	new
H	1589	1590	C=C stretch

Table 11: Raman Shift Frequencies and Proposed Assignments for RAK6 and MgRAK6

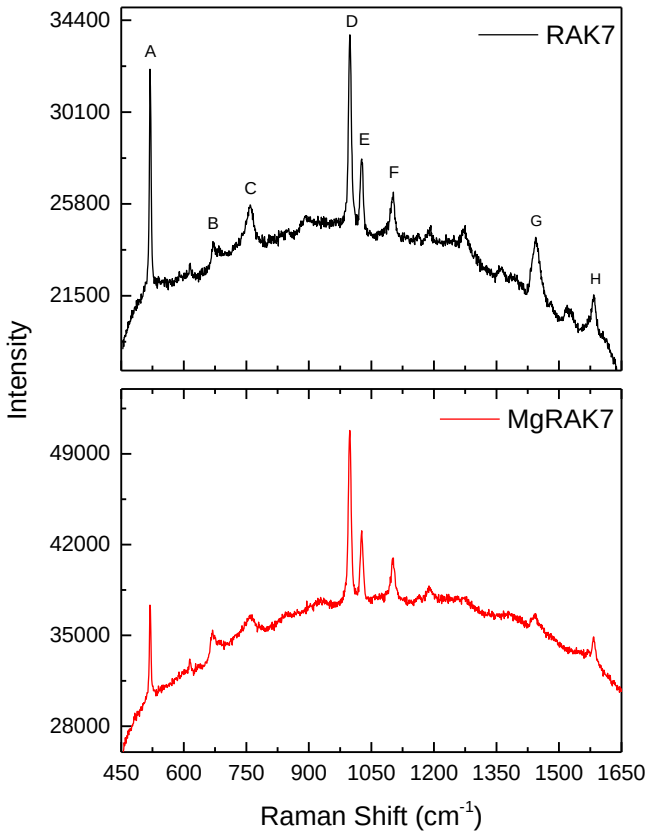

Figure 21: SERS Spectra Comparison between Ligand (RAK7) and Metal Ligand (MgRAK7) Complex

Peak Label	Ligand Raman Shift (cm^{-1})	Metal-Ligand Complex Raman Shift (cm^{-1})	Proposed Assignment
A	519	519	SiO_2 Substrate
B	670	669	
C	759	764	
D	998	998	Phenyl
E	1027	1027	Ring Breathing
F	1103	1103	
G	1445	1444	
H	1583	1583	C=C stretch

Table 12: Raman Shift Frequencies and Proposed Assignments for RAK7 and MgRAK7

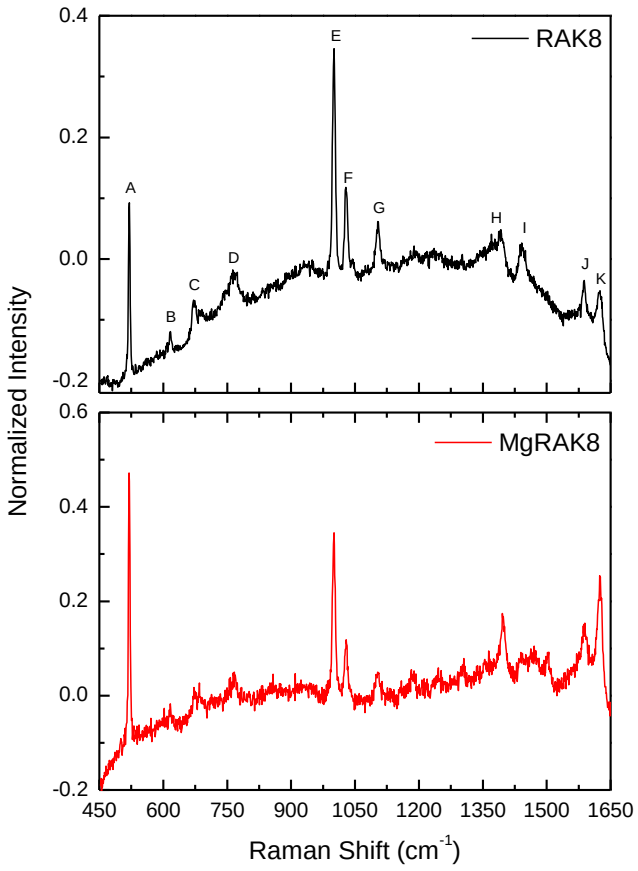

Figure 22: SERS Spectra Comparison between Ligand (RAK8) and Metal Ligand (MgRAK8) Complex

Peak Label	Ligand Raman Shift (cm^{-1})	Metal-Ligand Complex Raman Shift (cm^{-1})	Proposed Assignment
A	520	520	SiO_2 Substrate
B	616		
C	671	671	
D	763	767	
E	1001	1001	Phenyl
F	1028	1029	Ring Breathing
G	1104	1104	
H	1393	1396	
I	1441		
J	1588	1589	C=C stretch
K	1625	1624	C=N

Table 13: Raman Shift Frequencies and Proposed Assignments for RAK8 and MgRAK8

3.4.2.1. Low Concentration Samples

The spectra shown in Figure 23 have been measured from the MgRAK complexes at the lowest Mg concentration, as measured by ICP-MS. The concentrations are listed in Table 14 and the comparison of the key Raman modes are listed in Table 15. There are strong similarities in the SERS of the high and low concentration samples, validating the technique as applied to very low concentration samples.

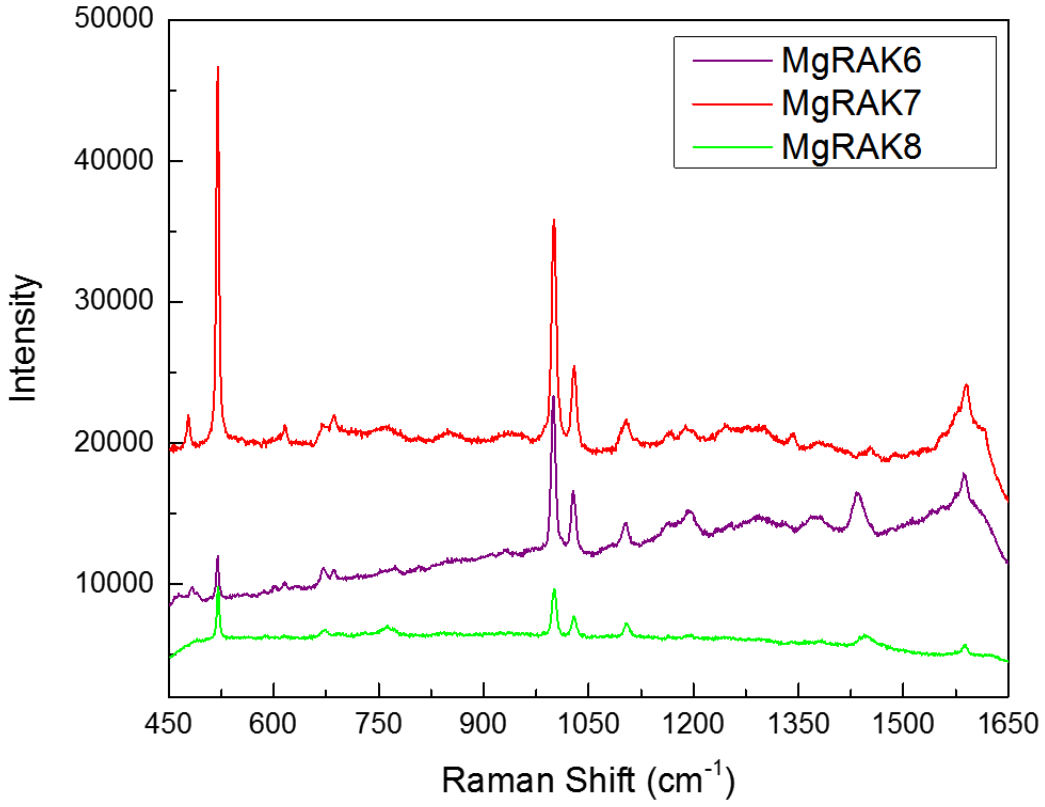

Figure 23: SERS Spectra of Lowest Measured Mg Concentration in Metal Ligand Complex-Loaded Proppants

	MgRAK6	MgRAK7	MgRAK8
[Mg] by ICP	6 ppm	7 ppm	8 ppm

Table 14: Mg Concentrations in Metal Ligand Complexes

Comparison Key Raman Shifts (cm^{-1})						
	MgRAK6		MgRAK7		MgRAK8	
Functional Group	223 ppm	6 ppm	62 ppm	7 ppm	230 ppm	8 ppm
Phenyl	1001	999	998	1001	1001	1001
Ring Breathing	1029	1027	1027	1029	1029	1029
C=C stretch	1105	1103	1103	1103	1104	1104
	1590	1588	1583	1590	1589	1588
C=N					1624	----

Table 15: SERS Comparison between High and Low Mg Concentration in Metal Ligand Complexes, Key Stretches

4. Discussion

Data obtained from the absorption studies of the aqueous ligands and their complexes confirm that complexes were formed due to the significant differences in their respective spectra, as shown in Figure 16, Figure 17, and Figure 18. The spectra of the metal complexes from Figure 16 (MgSalo-$PPh_3[Cl^-]_2$) and Figure 17 (MgSaloPh-$PPh_3[Cl^-]_2$) appear to shift to a shorter absorbance wavelength as compared to the spectrum of the metal complex in Figure 18 (MgSaloPy-$PPh_3[Cl^-]_2$), which appears to shift to a longer absorbance wavelength. In all cases, the absorbances were observed in the ultraviolet region and therefore support charge transfer occurring upon complexation. In addition to the higher and lower energy shifts measured, the disappearance of bands also support the complexation of the ligands to Mg metal.

Infrared spectroscopy data obtained from the Kemp research group also confirm that complexes were formed due to the significant absorbance peak differences measured for key vibrational modes involved with the ligand and metal coordination. These modes, C=N and C-O, show that for each complex formed, a change in the bond strength occurred due to the metal binding. The IR spectroscopy results are complementary to those of the UV-Vis spectroscopy in that the changes in vibrational modes measured are due to the proposed charge transfer transitions.

SERS data, however, do not show significant differences between the spectra of the ligand and of the complex. This can be attributed to the following reasons: (1) The salen-

type ligands are not highly polarizable and therefore have what is known as a small Raman cross-section that inherently does not produce strong signals. (2) Weak surface molecule interactions between the complexes and the plasmonic nanostructures that result in the reduced intensity of key vibrational modes that could otherwise be observed given electromagnetic enhancement is dependent on distance between plasmonic materials and the analyte. (3) The salen-type ligands contain various phenyl ring structures that dominate the spectra of other distinctive weaker vibrational modes such as C-O and possibly dominate stronger vibrational modes such as C=N. (4) The most straight forward modes involving the metal that can confirm complexation, Mg-O and Mg-C, are inherently weak.

Future work to address the aforementioned issues include using an excitation source that will overlap with both the electronic transition band of the molecule and the surface plasmon resonances to ensure the greatest signal enhancement. Alternatively, explore the possibility of modifying ligands and their complexes to achieve resonance with available excitation sources and the surface plasmon resonances. Other structure-based approaches include the modification of ligands and their complexes to improve adsorption onto the surface of the plasmonic nanostructures. Finally, investigate the possibilities of coordinating ligands with a range of larger metals that may lead to stronger characteristic vibrational modes.

5. Conclusion

In this work, a range of [O,N,N,O] tetradentate bis-Schiff bases were synthesized and investigated as potential subterranean fluid flow tracers by using Surface-Enhanced Raman Spectroscopy as the detection technique. These salen-type ligands and their metal complexes have been characterized by electronic and vibrational spectroscopic techniques and shown to be promising underground fluid flow tracers although structural modifications to the ligands and their complexes must be further investigated to support the intended application of this research. It has been demonstrated that the analysis of these ligands and their complexes by SERS establishes the ability of this technique to enhance the spectral signal although more work is needed to improve the technique's specificity of detection. This research represents an initial attempt at examining a unique chemical-based approach to subterranean fluid flow monitoring that may achieve improved efficiencies in future U.S. energy production. This research has demonstrated that SERS can potentially work as an identification technique for the above-ground detection of salen-type subterranean fluid flow tracers, pending optimization studies.

Appendix

Identification	Bridging group, Attached group	Molecular Structure
RAK0	Ethylene, t-Bu	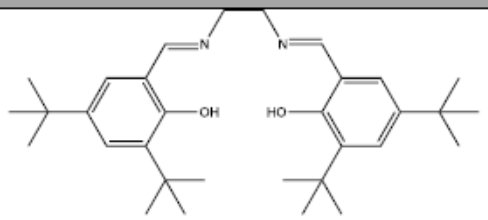
RAK1	Phenylene, t-Bu	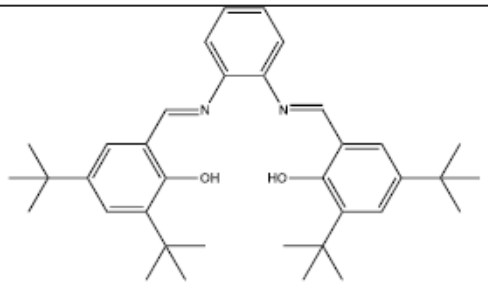
RAK2	Phenylene, Br	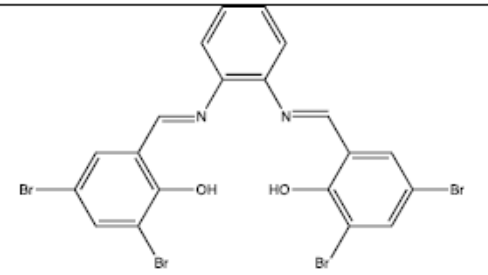
RAK3	Phenylene, -NO_2 groups	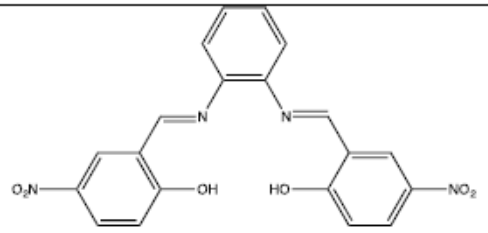
RAK4	Ethylene, Br	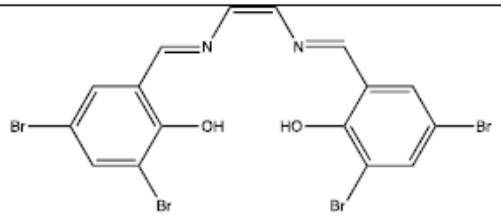

Table 16: List of Salen-Type Ligands Synthesized by the Kemp and Boyle Research Group Members, RAK1-4

RAK5	Ethylene, -NO_2 groups	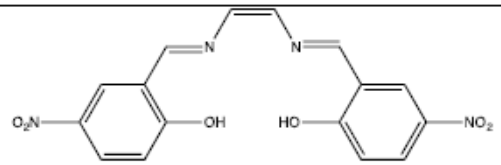
RAK6	Ethylene, ionic P^+ groups	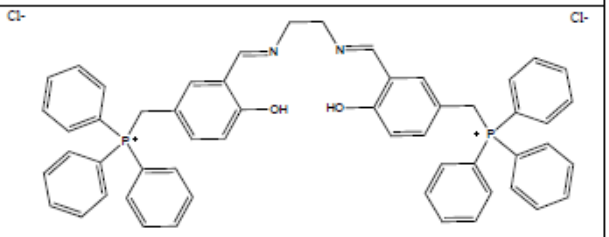
RAK7	Phenylene, ionic P^+ groups	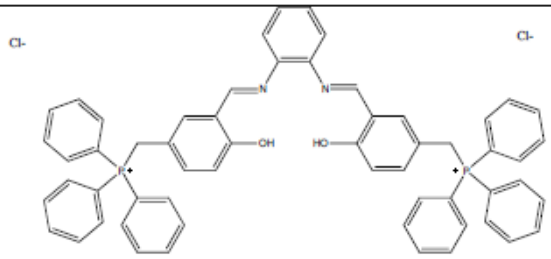
RAK8	Pyridine 5-coordinate, ionic P^+ groups	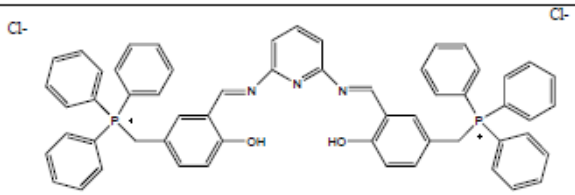

Table 17: List of Salen-Type Ligands Synthesized by the Kemp and Boyle Research Group Members, RAK5-8

References

(1) Administration, U. S. E. I. *Annual Energy Outlook 2018 with projections to 2050*, U.S. Energy Information Administration, 2018.
(2) Administration, U. S. E. I. *April 2017 Monthly Energy Review*, U.S. Energy Information Administration, 2017.
(3) U.S., E. P. A. 2018.
(4) Smith, R. G.; Maitland, G. C. *Trans IChemE* **1998**, *76*, 14.
(5) Hyman, J. D.; Jimenez-Martinez, J.; Viswanathan, H. S.; Carey, J. W.; Porter, M. L.; Rougier, E.; Karra, S.; Kang, Q.; Frash, L.; Chen, L.; Lei, Z.; O'Malley, D.; Makedonska, N. *Philosophical Transactions of the Royal Society a-Mathematical Physical and Engineering Sciences* **2016**, *374*.
(6) Serres-Piole, C.; Preud'homme, H.; Moradi-Tehrani, N.; Allanic, C.; Jullia, H.; Lobinski, R. *Journal of Petroleum Science and Engineering* **2012**, *98-99*, 22.
(7) National Academies of Sciences, E.; Medicine *Characterization, Modeling, Monitoring, and Remediation of Fractured Rock*; The National Academies Press: Washington, DC, 2015.
(8) Docherty, J.; Mabbott, S.; Smith, E.; Faulds, K.; Davidson, C.; Reglinski, J.; Graham, D. *Analyst* **2016**, *141*, 5857.
(9) Darensbourg, D. J.; Mackiewicz, R. M.; Rodgers, J. L.; Fang, C. C.; Billodeaux, D. R.; Reibenspies, J. H. *Inorganic Chemistry* **2004**, *43*, 6024.
(10) Cozzi, P. G. *Chemical Society Reviews* **2004**, *33*, 410.
(11) Atkins, P.; Overton, T.; Rourke, J.; Weller, M.; Armstrong, F. *Shriver & Atkins' Inorganic Chemistry*; 5th ed., 2010.
(12) Haikarainen, A.; Sipila, J.; Pietikainen, P.; Pajunen, A.; Mutikainen, I. *Journal of the Chemical Society-Dalton Transactions* **2001**, 991.
(13) Abd-Elzaher, M. M. *Synthesis and Reactivity in Inorganic and Metal-Organic Chemistry* **2000**, *30*, 1805.
(14) Bahramian, B.; Mirkhani, V.; Moghadam, M.; Amin, A. H. *Applied Catalysis A: General* **2006**, *315*, 52.
(15) Liang, F.; Sayed, M.; Al-Muntasheri, G. A.; Chang, F. F.; Li, L. *Petroleum* **2016**, *2*, 26.
(16) Diem, M. *Introduction to modern vibrational spectroscopy* Canada, 1993.
(17) Fox, M. *Optical Properties of Solids*; Oxford University: New York, 2001.
(18) Herzberg, G. *Molecular Spectra and Molecule Structure. I. Diatomic Molecules. By Gerhard Herzberg*; Krieger Publishing Company, 1940; Vol. I.
(19) Atkins, P.; de Paula, J. **2006**, 1085.
(20) Aroca, R. *Surface-Enhanced Vibrational Spectroscopy*; John Wiley & Sons Ltd: West Sussex, England, 2006.
(21) Smith, E.; Dent, G. *Modern Raman Spectroscopy - A Practical Approach*, 2005.
(22) Prochazka, M.; Springer International Publishing, 2016.
(23) Willets, K. A.; Van Duyne, R. P. *Annual Review of Physical Chemistry* **2007**, *58*, 267.
(24) Lombardi, J. R.; Birke, R. L. *Accounts of Chemical Research* **2009**, *42*, 734.
(25) Schlucker, S. *Angewandte Chemie-International Edition* **2014**, *53*, 4756.
(26) West, P. R.; Ishii, S.; Naik, G. V.; Emani, N. K.; Shalaev, V. M.; Boltasseva, A. *Laser & Photonics Reviews* **2010**, *4*, 795.
(27) Sharma, B.; Frontiera, R. R.; Henry, A.-I.; Ringe, E.; Van Duyne, R. P. *Materials Today* **2012**, *15*, 16.
(28) Mosier-Boss, P. A. *Nanomaterials* **2017**, *7*.

(29) Tesema, T. E.; Kafle, B.; Tadesse, M. G.; Habteyes, T. G. *Journal of Physical Chemistry C* **2017**, *121*, 7421.
(30) Staples, O. Senior Honors Thesis, University of New Mexico, 2017.
(31) Boyle Timothy, J. *Inorganic Chemistry* **2018**, *57*, 2402.
(32) Socrates, G. *Infrared and Raman Characteristic Group Frequencies: Tables and Charts*; 3rd ed.; John Wiley & Sons, Ltd: West Sussex, England, 2001.